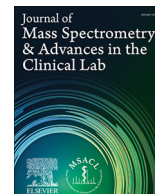




Contents lists available at ScienceDirect

Journal of Mass Spectrometry and Advances in the Clinical Lab

journal homepage: www.elsevier.com/locate/jmsacl

Research Article

Metabolomic and lipidomic characterization of an X-chromosome deletion disorder in neural progenitor cells by UHPLC-HRMS

Hoda Safari Yazd^a, Vanessa Y. Rubio^{a,b}, Casey A. Chamberlain^{c,d}, Richard A. Yost^a, Timothy J. Garrett^{c,*}^a Department of Chemistry, University of Florida, Gainesville, FL 32610, USA^b Department of Chemistry & Biochemistry, University of North Carolina at Greensboro, Greensboro, NC 27412, USA^c Department of Pathology, Immunology and Laboratory Medicine, University of Florida, Gainesville, FL 32610, USA^d Department of Chemistry, Washington University in St. Louis, St. Louis, MO 63130, USA

ARTICLE INFO

Article history:

Received 20 November 2020

Revised 5 May 2021

Accepted 24 May 2021

Available online 29 May 2021

Keywords:

Metabolomics

Lipidomics

Microdeletion

Xq27.3-Xq28

Fragile X syndrome

ABSTRACT

Introduction: Intellectual disorders involving deletions of the X chromosome present a difficult task in the determination of a connection between symptoms and metabolites that could lead to treatment options. One specific disorder of X-chromosomal deletion, Fragile X syndrome, is the most frequently occurring of intellectual disabilities. Previous metabolomic studies have been limited to mouse models that may not have sufficiently revealed the full biochemical diversity of the disease in humans.

Objectives: The primary objective of this study was to elucidate the human biochemistry in X-chromosomal deletion disorders through metabolomic and lipidomic profiling, using cells from a X-deletion patient as a representative case.

Methods: Metabolomic and lipidomic analysis was performed by UHPLC-HRMS on neural progenitor (NP) cells isolated from an afflicted female patient versus normal neural progenitor cells.

Results: Results showed perturbations in several metabolic pathways, including those of arginine and proline, that significantly impact both neurotransmitter generation and overall brain function. Coincidentally, dysregulation was observed for lipids involved in both cellular structure and membrane integrity. The trends of observed metabolomic changes, as well as lipidomic profiling from identified features, are discussed.

Conclusion: The lipidomic and metabolomic profiles of NP cell samples exhibited significant differentiation associated with partial deletion of the X chromosome. These findings suggest that rare X-chromosomal deletion disorders are not only a mental disorder limited to alterations in local neuronal functions, but are also metabolic diseases.

© 2021 THE AUTHORS. Publishing services by ELSEVIER B.V. on behalf of MSACL. This is an open access article under the CC BY-NC-ND license (<http://creativecommons.org/licenses/by-nc-nd/4.0/>).

1. Introduction

Mutations in the X chromosome are responsible for hundreds of inherited intellectual disabilities whose associated diseases primarily affect males and can have extremely variable clinical manifestations. However, a subset of X chromosome-associated diseases, including Fragile X, Rett (RTT), Turner, Hunter, and CDKL5 syndromes also affect females [1,2]. Partial or complete deletion of

the X chromosome is a rare condition that causes a variety of possible maladies, including autism, seizures, constipation, drooling, and chronic sinusitis, with the severity of the condition approximately corresponding to genotype and the amount of X chromosome disruption [3,4].

Metabolomics, the comprehensive study of small molecules that are consumed or produced by various cellular processes in a given biological sample, is an emerging discipline that explores detailed snapshots of metabolic profiles [5,6]. Lipidomics has been defined as a subset of metabolomics, associated specifically with lipid analysis, which aims to comprehensively and quantitatively describe all lipid (typically hydrophobic) species present in a sample [7]. Lipid and small metabolite abundances in biological specimens are directly related to pathogenic mechanisms, which makes them reporters for various human diseases [8]. As metabolomics provides the simultaneous measurement of many small

Abbreviations: BMP, Bis(monoacylglycerol) phosphate; Cer-NS, Ceramide non-hydroxyfatty acid-sphingosines; HexCer-NS, Hexosylceramide nonhydroxyfatty acid-sphingosines; GL, Glycerolipid; LPC, Lysophosphatidylcholines; PC, Phosphatidylcholine; PG, Phosphatidylglycerol; PE, Phosphatidylethanolamine; SM, Sphingomyelin; SP, Sphingolipid; ST, Sterol.

* Corresponding author.

E-mail address: tgarrett@ufl.edu (T.J. Garrett).

<https://doi.org/10.1016/j.jmsacl.2021.05.002>

2667-145X/© 2021 THE AUTHORS. Publishing services by ELSEVIER B.V. on behalf of MSACL.

This is an open access article under the CC BY-NC-ND license (<http://creativecommons.org/licenses/by-nc-nd/4.0/>).

molecule metabolites and lipids in a given physiological or pathological condition, subtle changes in the expression level of a gene or protein can result in significant variations in the downstream metabolites that can lead to mechanistic elucidation or biomarker discovery and, ultimately, new therapeutic strategies [9]. The combination of lipidomic and metabolomic analyses provides a comprehensive atlas of the metabolic landscape and a measure of functional biological phenotype. These data permit in-depth pathway analysis to identify significant metabolic drivers in disease pathology and identify biomarkers related to the prognosis or diagnosis of a range of diseases. The application of such a methodology to the analysis of a rare X-chromosomal deletion (X-deletion) syndrome has the potential to illustrate its metabolomic and lipidomic signatures.

Several metabolomic studies have been conducted on a variety of X-linked intellectual disabilities such as the Fragile X syndrome (FXS), which is the most frequent cause of inherited intellectual disability, Turner syndrome, and a variety of other models, to understand the dysregulation of metabolic pathways in rare X-deletion disorders [10–13]. In previous metabolomic studies on FXS, it was found that FXS led to disturbances in purine and pyrimidine metabolism, which suggested that these features could be targeted as treatment options to offset this pathological effect. The compound suramin, a competitive inhibitor of purinergic signaling, was employed as a treatment, and led to an improvement of symptoms in the FXS (FMR1 knockout) mouse model. Suramin was shown to alter 20 out of 60 metabolic pathways investigated, indicating the broad scope of off-target effects a drug can have on metabolic pathways (pharmacometabolism) [10]. Additionally, the FXS mouse model studies revealed that neurotransmitter levels, osmoregulation, energy metabolism, and oxidative stress responses are perturbed in this syndrome. This research showed that FXS and X-deletion disorders can affect several neurotransmitters and the readjustment of brain biochemical pathways [11].

Human studies are essential in helping to understand the metabolic signatures of rare X-deletion disorders. However, while previous studies have been primarily performed in mouse models, few metabolomic studies on these disorders have been conducted using human-derived samples. In this study, neural progenitor (NP) cells were differentiated from the plasma of a subject afflicted with X-deletion for the unique opportunity to perform metabolomics on human cells. NP cells are of high importance for understanding X-deletion disorders as they affect neurological metabolism. These cells recapitulate early brain developmental events and are, thus, invaluable for studying the neurobiology of inherited neurological disorders [14,15]. Unlike neural cells, NP cells can be cultured and provide cost-efficient access to large cell volumes for metabolomic and lipidomic analyses.

To better describe the rare X-deletion syndrome and capture its biochemical signature in human NP cells, we performed untargeted profiling of the metabolome and lipidome on the clones of NP cells with X-deletion and the clones expressing the normal X chromosome using ultra high-performance liquid chromatography-high-resolution mass spectrometry (UHPLC-HRMS). Subsequent multivariate statistical analyses were used to characterize interconnected differential metabolites and lipids and identify the specific pathway alterations associated with X-deletion syndrome. The overall metabolomic and lipidomic analysis workflow that was performed in this study is summarized in Scheme 1. The critical differential features of X-deletion syndrome derived from this study may subsequently open new diagnostic paradigms and be evaluated as candidate metabolic treatment options for rare X-deletion disorders.

2. Materials and methods

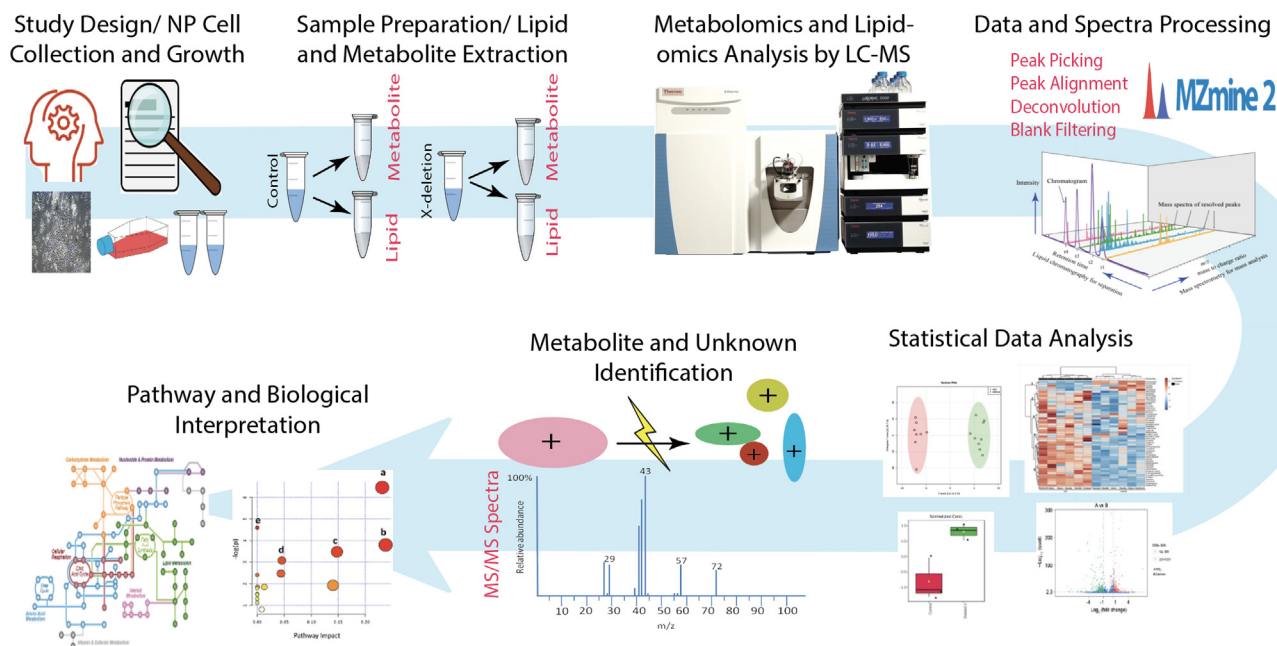
2.1. Chemicals and reagents

LC-MS grade acetonitrile (ACN), water with 0.1% formic acid, 2-propanol (IPA), and all other analytical-grade solvents including methanol (MeOH), chloroform (CHCl_3), ammonium acetate, and ammonium formate were purchased from Thermo Fisher Scientific (Waltham, MA). Lipid internal and injection standards were purchased from Avanti Polar Lipids, Inc. (Alabaster, AL) and metabolite internal and injection standards were purchased from CDN Isotopes (Pointe-Claire, Quebec, Canada), Acros Organics (Fair Lawn, NJ), and Cambridge Isotope Laboratories, Inc. (Tewksbury, MA). For the establishment of patient-derived induced pluripotent stem cells (iPSC), SepMate tubes, Lymphoprep, ReproTeSR, and ReLeSR medium were purchased from StemCell Technologies (Vancouver, Canada), 6-well plates coated with Corning Matrigel hESC-qualified Matrix were purchased from Corning (Corning, NY), and dihydrochloride was purchased from Tocris Bioscience (Bristol, UK). For generating and culturing NP cells, mTeSR 1 medium, STEMdiff Neural Induction Kit, STEMdiff Neural Progenitor Medium, and Accutase were purchased from STEMCELL Technologies (Vancouver, Canada). Y-27632 (ROCK inhibitor) was purchased from SelleckChem (Houston, TX), DPBS (Gibco) from Thermo Fisher Scientific and DMEM/F12 with HEPES from Corning (Corning, NY).

2.2. Patient information and establishment of patient-derived iPSCs

The patient was diagnosed with a 7.3 megabase deletion at Xq27.3q28 (142,271,441–149,561,309 bp). This X chromosomal deletion emerged in hemizygoty for 76 RefSeq genes, including OMIM (online mendelian inheritance in man) disease-associated genes like AFF2, FMR1, and IDS genes, which are correlated with fragile XE syndrome, FXS, and Hunter syndrome, respectively.

To establish iPSCs from the patient, approximately 5 mL of the patient's peripheral blood was collected into an EDTA tube. Utilizing SepMate tubes and Lymphoprep, peripheral blood mononuclear cells (PBMCs) were isolated. A total of 4×10^5 PBMCs were suspended in blood growth medium (RPMI 1640, 10% fetal bovine serum, and 1% penicillin–streptomycin solution) and infected with Sendai viral vector SeVdp (KOSM) 302L encoding four reprogramming factors (Oct4, Sox2, Klf4, and c-Myc) with a multiplicity of infection of 2 at 37 °C for 2 h. Using 6-well plates coated with Corning Matrigel hESC-qualified Matrix, the cells were seeded at 2×10^5 cells per well. The cells were cultured for the first three days in blood growth medium and then transferred to ReproTeSR medium until iPSC colonies were available for isolation. Nearly three weeks after the viral infection, individual iPSC colonies were manually isolated and transferred into Matrigel-coated dishes in 10 μM Y-27632 dihydrochloride supplemented TeSR1 medium. The cells were kept in mTeSR1 medium with daily medium changes and passaged every six days using ReLeSR. 11 clones of iPSCs were established and RNA expression of these 11 clones were examined using quantitative RT-PCR (Reverse Transcription-Polymerase Chain Reaction). Due to random X chromosome inactivation, five clones among the 11 clones expressed the deleted abnormal X chromosome, while the remaining six clones expressed the normal X chromosome. NP cells were established, as summarized in the following section, from the former and latter clones, which were used as the X-deletion and control NP cells in this study, respectively. Watanabe et al. comprehensively explained the establishment process of patient-derived iPSCs [16].



Scheme 1. Overview of LC-HRMS metabolomics and lipidomic workflows employed in this research. Metabolites and lipids were extracted from the NP cell sample matrix. Separate chromatographic methods were applied to metabolites and lipids, followed by electrospray ionization and analysis using HRMS. After data and spectra evaluation and multivariate and univariate statistical analysis, features of interest were selected from the data and identified using the *in-house* library, MS/MS, and database searches. Identified compounds were then used for metabolic impact and pathway analysis, and biological interpretation.

2.3. Cell culture

NP cells were differentiated from the iPSCs according to the following procedure. For preparing the medium, 0.5 mL of STEMdiff SMADi Neural Induction Supplement was added to 250 mL of STEMdiff Neural Medium. Firstly, iPSC single cells were plated in a coated 6-well plate with matrigel by culturing them with 2 mL/well mTeSR 1 medium and 1 mL of accutase. After incubation for 8–10 min at 37 °C, the cells were pipetted until they were separated into single cells, after which they were transferred to a tube and centrifugated for 5 min at 300 × g. The supernatant was resuspended in 1 mL of Neural Induction Medium + ROCKi (10 μM), and, finally, the cells were plated at the desired density (2 × 10⁶ cells/well) in 2 mL of Neural Induction Medium + ROCKi in a single well of a new matrigel-coated 6-well plate and incubated at 37 °C. Over the next 6 days, the medium was changed daily with 2 mL of Neural Induction Medium (+SMADi). The cells were passaged at 80–90% confluency using the following steps. First, the cells were dissociated by pipetting and transferred to a conical 15 mL tube containing 3 mL of DMEM/F12 followed by centrifugation at 300 × g for 5 min. Next, the supernatant was resuspended in 1 mL of Neural Induction Medium (with SMADi) + ROCKi (10 μM) and plated at the desired density (1.2 × 10⁶ cells/well) in 2 mL of Neural Induction Medium (with SMADi) + ROCKi in a single well of a new 6-well plate and incubated at 37 °C. When cells were ready for passage 3, the medium was switched from Neural Induction Medium to STEMdiff Neural Progenitor Medium. To confirm the active status of either the X-deletion or normal X chromosome in final NP cells, expression levels of FMR1 and other X chromosomal genes were validated. The X-deletion NP cells from the patient expressed an undetectable level of the FMR1 gene, and in contrast, the control NP cells from the patient expressed a normal level, which was equivalent to NP cells derived from a healthy individual [16]. After several passages, the cells in both control and X chromosomal deletion groups were collected and counted using trypan blue and a hemocytometer

(1 × 10⁷ cells per sample). Cells were stored at –80 °C until needed for metabolite and lipid extraction.

2.4. Metabolomics analysis sample preparation

Metabolites were extracted using 1 × 10⁷ cells per group (cell count used for pre-data acquisition normalization). To preserve sample quality, samples were kept on ice and out of UV light at all steps whenever possible. Cells were pelleted by 5 min of centrifugation at 445×g and 4 °C, then washed by adding 1 mL of 40 mM ammonium formate in water. This step was repeated two additional times, discarding the supernatant after each wash. Cells were then resuspended in 50 μL of 5 mM ammonium acetate in water and homogenized with 0.7 mm zirconia beads for 30 s at 1800 rpm using a bead beater (FastPrep-96, MP Biomedicals). The samples were then incubated on ice for 15 min. The homogenization procedure was repeated two more times. Then, 25 μL from each homogenized sample was transferred to a polypropylene tube and 2 μL of an internal standard mixture in 0.1% formic acid in water containing tryptophan-2,3,3-D3 (40 μg/mL), propionic acid-13C3 (8 μg/mL), creatine-D3 (8 μg/mL), leucine-D10 (4 μg/mL), tyrosine-13C6 (4 μg/mL), leucine-13C6 (4 μg/mL), phenylalanine 13C6 (8 μg/mL), N-BOC-*tert*-leucine (4 μg/mL), caffeine-D3 (4 μg/mL), N-BOC-aspartic acid (4 μg/mL), succinic acid-2,3,3,3-D4 (4 μg/mL), salicylic acid-D6 (4 μg/mL). The samples were then vortex mixed. Next, 500 μL ice-cold 80% methanol was added to induce protein precipitation. Samples were mixed for 30 s at 1800 rpm using a bead beater followed by incubation in the refrigerator (4 °C) for 30 min to allow for further protein precipitation. The samples were centrifuged at 445×g for 5 min at 4 °C to pellet the proteins and the supernatants (500 μL) containing metabolite content of the cells were transferred to a new tube and dried under nitrogen gas at 30 °C. Finally, the samples were reconstituted in 25 μL of 0.1% formic acid in water containing the following injection standards (BOC-L-tyrosine, N-alpha-BOC-tryptophan, and BOC-phenylalanine (all at 2 μg/mL)). Samples were vortex mixed

and incubated on ice for 15 min, then centrifuged at 445×g for 5 min at 4 °C to pellet any remaining debris. The supernatants were transferred to glass LC vials with fused inserts for analysis.

2.5. Lipidomics analysis sample preparation

Similar to metabolite extraction, the cells in each sample were pelleted, washed, and homogenized. The lipids were extracted using a modified version of the Folch method [17]. First, 25 µL from each homogenized sample was transferred to a new glass vial and 5 µL of internal standard mixture containing lysophosphatidylcholine (LPC) 17:0, phosphatidylserine (PS) 14:0/14:0, phosphatidylcholine (PC) 17:0/17:0, phosphatidylglycerol (PG) 14:0/14:0, phosphatidylethanolamine (PE) 15:0/15:0, phosphatidylinositol (PI) 8:0, sphingomyelin (SM) d18:1/17:0, ceramide (Cer) d18:1/17:0, diacylglycerol (DG) 14:0/ 14:0, triacylglycerol (TG) 15:0/15:0/15:0, cardiolipin (CL) 15:0(3)-16:1, bis(monacylglycerol)phosphate (BMP) 14:0 (S,R), 1-palmitoyl-2-azelaoyl-sn-glycero-3-phosphocholine (PAzePC), Cer(Glycosyl(β) C12, sphingosine(d17:1), Glucosyl(β) C12 Cer, Lyso SM(d17:1) each at 100 ppm in 2:1 chloroform: methanol was added, followed by vortex mixing. Next, 100 µL of ice-cold methanol and 200 µL of ice-cold chloroform were added to each vial. The samples were incubated at 4 °C for 20 min and vortex mixed every 10 min. Then, 50 µL of water was added, and the samples were vortex mixed and again incubated at 4 °C for 10 min and vortex mixed after 5 min. The aqueous and organic layers were separated by centrifuging at 3260×g and 4 °C for 10 min. Then, 240 µL of the bottom organic layer containing the lipids was transferred to a new glass vial and cooled on ice. The aqueous layer was re-extracted by adding 100 µL of ice-cold 2:1 chloroform: methanol, followed by vortex mixing and incubating on ice for 10 min. After centrifugation of samples at 3260×g and 4 °C for 10 min, another 80 µL sample from the second organic layer was removed and combined with the first organic layer. Finally, lipid extracts were dried under nitrogen gas at 30 °C and reconstituted in 30 µL of IPA containing injection standards (1000 ppm of: LPC(19:0), PC(19:0/19:0), PG(17:0/17:0), PE (17:0/17:0), PS(17:0/17:0), TG(17:0/17:0/17:0)). To remove any debris, the samples were centrifuged at 3260×g for 10 min at 4 °C and the supernatant was transferred to glass LC vials with micro inserts. For quality control, extraction blanks and reconstitution blanks were also prepared.

2.6. Data acquisition method

All lipidomic and metabolomic analyses were performed on a Q Exactive Orbitrap Mass Spectrometer with heated electrospray ionization coupled to a Dionex Ultimate 3000 UHPLC system (Thermo Fisher Scientific) in both positive and negative ion modes (metabolomics source settings: spray voltage = 3500 V (+mode) and 3000 V (– mode), aux gas = 10, sheath gas = 50, capillary temperature = 325 °C, spray gas = 1, and S-lens RF level = 30/ Lipidomics source settings: spray voltage = 3500 V, aux gas = 5 (+ mode) and 15 (– mode), sheath gas = 30 (+ mode) and 25 (– mode), capillary temperature = 300 °C, spray gas = 1 (+ mode) and 0 (– mode), and S-lens RF level = 35). Samples were kept at 8 °C in the autosampler.

For lipidomics, an AQUITY UPLC BEH C18 column (1.7 µm, 2.1 mm × 50 mm) with corresponding VanGuard pre-column (Waters Corporation, Milford, MA, USA) maintained at 50 °C was used. Mobile phase C was 60:40 ACN:water with 0.1% formic acid and 10 mM ammonium formate in water, and mobile phase D was 90:8:2 IPA:ACN:water with 0.1% formic acid and 10 mM ammonium formate in water. Stepwise gradient elution was ramped from 20% D to 98% D with a 0.5 mL/min flow rate over 17.00 min followed by 3.00 min column flush and re-equilibration (see

Table S1 for exact step conditions). The total runtime with equilibration was 23.00 min (injection volume was 3 µL for positive polarity and 5 µL for negative polarity). Mass spectra were acquired in full scan mode (70,000 mass resolution), data-dependent MS/MS mode (35,000 mass resolution, top 5), and all-ion fragmentation MS/MS mode (70,000 mass resolution) from 200 to 2200 *m/z*. Triplicate full scan injections were conducted on each sample. Data-dependent iterative exclusion acquisition (ddMS2 – IE, IE-omics) was performed using an automated exclusion list generated between runs to increase detection coverage of lower intensity lipid species and improve identifications during lipidomic analysis [18]. For IE-omics and in positive ion mode data, a total of five iterative injection rounds were analyzed, and in negative ion mode, a total of three iterative injections rounds were analyzed at 35,000 mass resolution. In addition, data-dependent MS/MS mode (35,000 mass resolution) was carried out on 9 selected unknown lipid mass features.

For metabolomic analysis, an ACE-Excel 2 C18-Pentafluorophenyl column (2 µm, 2.1 mm × 100 mm) (Advanced Chromatography Technologies Ltd., Aberdeen, Scotland) maintained at 25 °C was used. Mobile phase A was 0.1% formic acid in the water and mobile phase B was ACN. Reverse phase gradient elution was ramped from 0% B to 80% B over 13.0 min at 350 µL/min, which increased to 600 µL/min between 16.80 and 17.50 min for column flush and re-equilibration (see Table S2 for full conditions). The total runtime was 20.50 min, and data were acquired in both positive and negative ion modes (injection volume was 2 µL for positive polarity and 4 µL for negative polarity) in full scan mode (35,000 mass resolution) and data-dependent MS/MS mode (17,500 mass resolution) from 70 to 1000 *m/z*. Triplicate full scan injections were conducted on each sample.

2.7. Data processing

The performance of spiked injection and internal standards in all samples was checked and qualified as showing a relative standard deviation of less than 10% to monitor the quality of the data and check the reproducibility in the analysis. For metabolomic data analysis, data files were converted to .mzXML format from .RAW format using RawConverter [19], and MZmine 2 [20] was employed for feature detection, peak picking, chromatographic alignment, and metabolite identification using our method-specific library based on *m/z* (ppm window in positive mode = 5 ppm and negative mode = 10 ppm) and retention time matching (RT window = +/-0.25 min) (Metabolomics Standards Initiative Level 1 Identification) [21]. LipidMatch Flow software was used for all lipidomic data analysis processing, including file format conversion, peak picking, chromatographic alignment, and lipid identification (which is based on MS/MS fragmentation spectral matching to in silico databases) [22].

2.8. Statistical analysis

Statistical analysis was performed using MetaboAnalyst 4.0 [23] with the following parameters: (1) peak intensity data, (2) samples in rows unpaired, (3) missing value estimation used to replace by a small value (half of the minimum positive value in the original data, none of the features were removed in this step), (4) normalized to sum (to correct the instrumental and the technical variation), (5) data transformed using log transformation, and (6) autoscaled (to allow a more direct comparison between features of greatly varying intensities). Principal component analysis (PCA), an unsupervised statistical model, was employed to visualize variance and emphasize variation in both metabolomic and lipidomic analysis. Heatmaps (hierarchical clustering analysis based on Student's *t*-test) were generated using Python 3 Seaborn

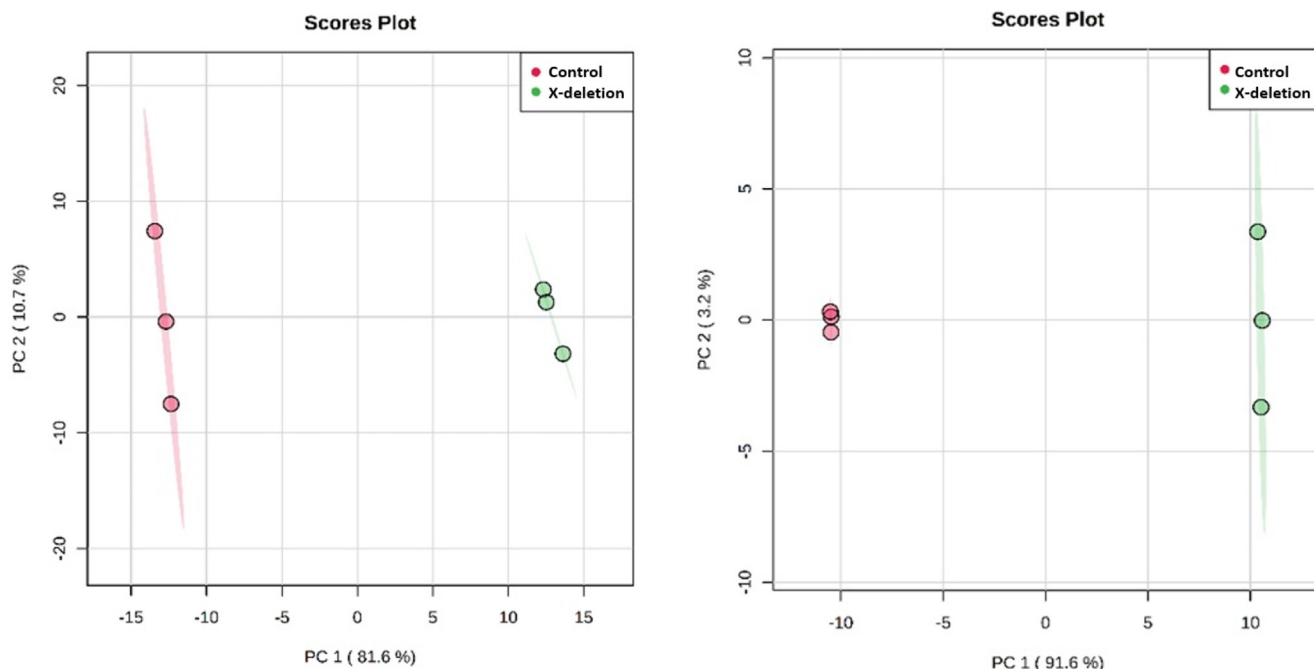


Fig. 1. Principal component analysis (PCA) was constructed using lipidomics data and could separate the samples when plotted against the first two principal components (Left: positive ion mode, Right: negative ion mode).

Table 1

Mean peak height (PH) of significantly different lipids in X-deletion sample injections ($n = 3$) compared to control sample injections ($n = 3$) and their ratio in positive mode (ID methods: 1 = More than one MS/MS fragment m/z match to in silico database from data dependent (top 5), 2 = all-ion fragmentation MS/MS fragment m/z match, 3 = Only one fragment m/z match).

Lipid Name	m/z	Ion/ Adduct	ID methods	Mass Accuracy (ppm)	Average X-deletion PH ($n = 3$)	X-deletion RSD (%)	Average Control PH ($n = 3$)	Control RSD (%)	X-deletion/ Control
PC(38:6)	792.5903	[M+H] ⁺	3	-0.5	6.40E+05	3.47	1.27E+04	52.65	50.5
PE(40:8)	788.5264	[M+H] ⁺	3	4.3	2.37E+05	4.33	9.71E+03	26.77	24.4
Plasmenyl-PC(P-16:0/20:4)	766.5755	[M+H] ⁺	1,2	1.3	1.28E+08	20.3	5.97E+06	2.81	21.4
PC(38:7)	790.5743	[M+H] ⁺	3	-1	4.63E+06	2.98	2.83E+05	12.88	16.3
BMP(18:2_20:3)	814.5615	[M+H] ⁺	2	2.8	2.97E+05	0.84	1.83E+04	23.14	16.2
HexCer-NS(d18:1/17:0)	714.5894	[M+H] ⁺	1	2.2	5.57E+05	10.51	3.72E+04	18.16	15
Plasmenyl-PC(P-18:1/20:4)	792.5911	[M+H] ⁺	1	0.3	7.55E+07	6.85	5.19E+06	6.87	14.5
PC(40:7)	818.6067	[M+H] ⁺	3	0.4	8.62E+05	9.59	6.03E+04	18.22	14.3
LPC(18:1)	506.3627	[M+H] ⁺	3	-3.2	5.55E+05	10.28	5.02E+04	9.94	11.1
BMP(18:2_22:4)	840.577	[M+H] ⁺	1,2	2.5	5.14E+06	2.84	4.86E+05	2.91	10.6
Plasmenyl-PC(P-16:0/22:4)	794.6061	[M+H] ⁺	1	0.4	3.28E+07	5.28	3.40E+06	6.69	9.65
Plasmenyl-PC(P-18:0/20:4)	794.6055	[M+H] ⁺	1,2	-0.3	2.46E+07	5.91	2.58E+06	4.07	9.55
BMP(18:2_20:4)	812.5456	[M+H] ⁺	1	2.5	5.43E+05	0.19	5.71E+04	3.04	9.5
PC(36:5)	780.5921	[M+H] ⁺	3	-2.8	1.63E+06	44.43	1.78E+05	4.85	9.2
PC(34:5)	752.5256	[M+H] ⁺	3	3.4	5.26E+05	7.02	6.21E+04	32.34	8.5
TG(18:1_18:1_20:4)	924.804	[M+NH ₄] ⁺	1	2.8	1.23E+06	3.86	1.47E+05	0.44	8.4
PC(38:4)	796.622	[M+H] ⁺	3	0	9.43E+06	1.46	1.15E+06	4.52	8.2
PC(40:6)	820.6216	[M+H] ⁺	3	-0.5	3.85E+06	4.3	4.87E+05	3.29	7.9
Plasmenyl-PC(P-18:1/22:4)	820.6225	[M+H] ⁺	1	1.3	1.93E+07	4.5	2.54E+06	5.5	7.6

to visualize metabolite and lipid intensity differences between the two samples generated from both positive and negative ion mode data [24]. We defined significance with a p -value cut-off of ≤ 0.005 in this study.

2.9. Pathway enrichment analysis

For lipidomic pathway analysis, Lipid Ontology (LION) enrichment analysis was used [25], and a one-tailed Student's t -test was employed to rank input identifiers. For metabolomic pathway analysis, enrichment analysis module, and pathway analysis module on Metaboanalyst 4.0 was applied [23]. The differential

metabolites of X-deletion and control samples with a p -value smaller than 0.05 were imported to these modules matching the Human Metabolome Database, PubChem, and KEGG databases. The pathway network was manually constructed based on the KEGG pathway matching [26–33].

3. Results and discussion

3.1. Lipidomics analysis

Global lipidomics analysis on control and X-deletion samples generated 1507 features in positive ion mode and 580 features

Table 2

Mean peak height (PH) of significantly different lipids in X-deletion sample injections (n = 3) compared to control sample injections (n = 3) and their ratio in negative mode (ID methods: ID methods: 1 = More than one MS/MS fragment *m/z* match to in silico database from data dependent (top 5), 2 = all-ion fragmentation MS/MS fragment *m/z* match).

Lipid Name	<i>m/z</i>	Ion/Adduct	ID methods	Mass Accuracy (ppm)	Average X-deletion PH (n = 3)	X-deletion RSD (%)	Average Control PH (n = 3)	Control RSD (%)	X-deletion/Control
PG(20:3_20:3)	821.5358	[M-H] ⁻	1,2	2.5	2.76E+06	1.79	9.64E+04	5	28.7
PG(18:1_20:4)	795.5199	[M-H] ⁻	1,2	2.3	9.93E+06	0.61	6.08E+05	9.4	16.3
Plasmanyl-PC(O-16:1/20:4)	810.5674	[M+HCO ₂] ⁻	1	2.4	1.28E+07	0.9	8.59E+05	1.62	15
PG(18:2_20:3)	795.5200	[M-H] ⁻	1,2	3.1	3.72E+05	1.94	2.90E+04	14.78	12.8
Plasmanyl-PC(P-18:1/20:4)	836.5830	[M+HCO ₂] ⁻	1	2.3	8.14E+06	0.63	6.83E+05	3.98	11.9
Plasmanyl-PC(O-18:1/20:4)	838.5981	[M+HCO ₂] ⁻	1	1.6	2.19E+06	2.67	1.85E+05	6.41	11.9
Plasmanyl-PC(O-16:1/22:4)	838.5975	[M+HCO ₂] ⁻	1	0.1	3.72E+06	2.96	4.13E+05	4.5	9.02
PG(20:4_20:4)	817.5049	[M-H] ⁻	2	3	5.31E+05	3.85	6.31E+04	1.28	8.41
Plasmanyl-PC(O-16:1/20:3)	812.5826	[M+HCO ₂] ⁻	1	1.9	9.60E+05	2.24	1.21E+05	7.05	7.95
Plasmanyl-PC(P-18:1/22:4)	864.6134	[M+HCO ₂] ⁻	1	1.2	1.97E+06	3.46	2.53E+05	21.71	7.78

in negative ion mode datasets. After identification by MS/MS fragmentation using LipidMatch flow [22], 227 features were identified in positive and 144 features were identified in negative ion mode. Subsequent analysis in positive mode resulted in 9 additional features by MS/MS using CFM-ID 3.0 [34]. Unidentified features were discarded, as many of these unknown features may be contamination, MS artifacts, and isomeric overlap peaks that are not related to the biological sample [35]. Only the identified features were used for statistical analysis. Initially, PCA was applied to positive and negative ion mode datasets separately to observe the differences between the control and X-deletion groups. The results showed primary separation of the two groups along PC1, explaining 92.3% of the variance in 2 PCs in positive and 94.8% of the variance in negative ion mode (Fig. 1). Table 1 displays the top 19 significantly identified lipids with fold changes greater than 7.5 in positive ion mode (to only look at the lipids with the highest magnitude of change), and Table 2, shows the top 10 significantly identified lipids with fold changes greater than 7.5 in negative ion mode (Table S3 presents the

other possible identification of lipids in Tables 1 and 2 caused by the high degree of overlap in lipid identification using MS/MS). The representative extracted ion chromatograms (EICs) for one selected significant lipid in positive (PC(40:7)) and one in negative ion mode (PG(20:3_20:3)) between X-deletion and control samples are shown in Fig. 2 with their associated mass spectra to show that clear differences were observed.

A heatmap was generated by performing hierarchical clustering analysis on the positive ion mode dataset, providing a visual representation of the top 50 significant lipids based on the Student's *t*-test analysis and how their intensity varies between the groups (Fig. 3). The same results for negative ion mode are shown in Fig. S1. Shades of yellow and purple represent an increased or decreased fold change, respectively, of lipids in X-deletion relative to control. Significant hierarchical clustering groups were observed among the cells between both groups. As is evident in Tables 1, 2, and Fig. 3, phosphatidylcholine (PC) and phosphatidylethanolamine (PE) lipids showed the greatest representation amongst the significantly altered lipids. PCs are the primary

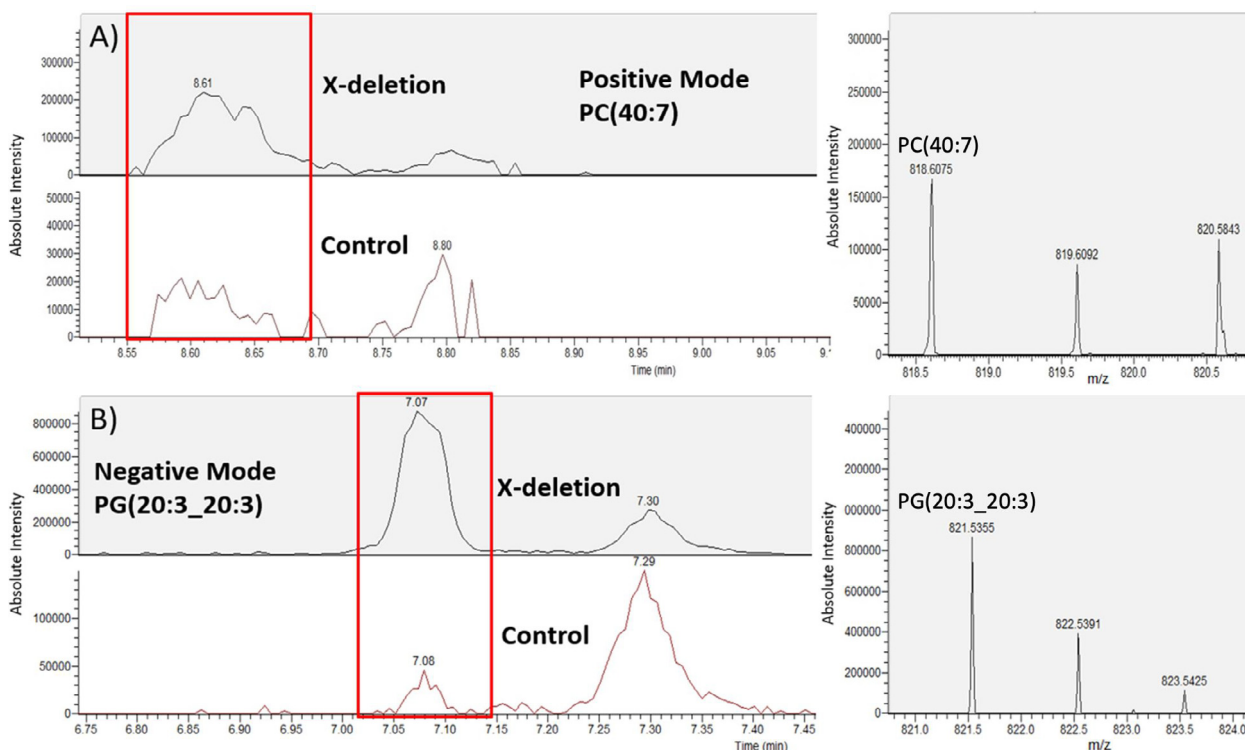


Fig. 2. Representative Extracted Ion Chromatogram (XIC) and mass spectra of two lipids isolated from the control sample and X-deletion sample based on UHPLC/MS in electrospray ionization (ESI) in A) Positive and B) Negative mode.

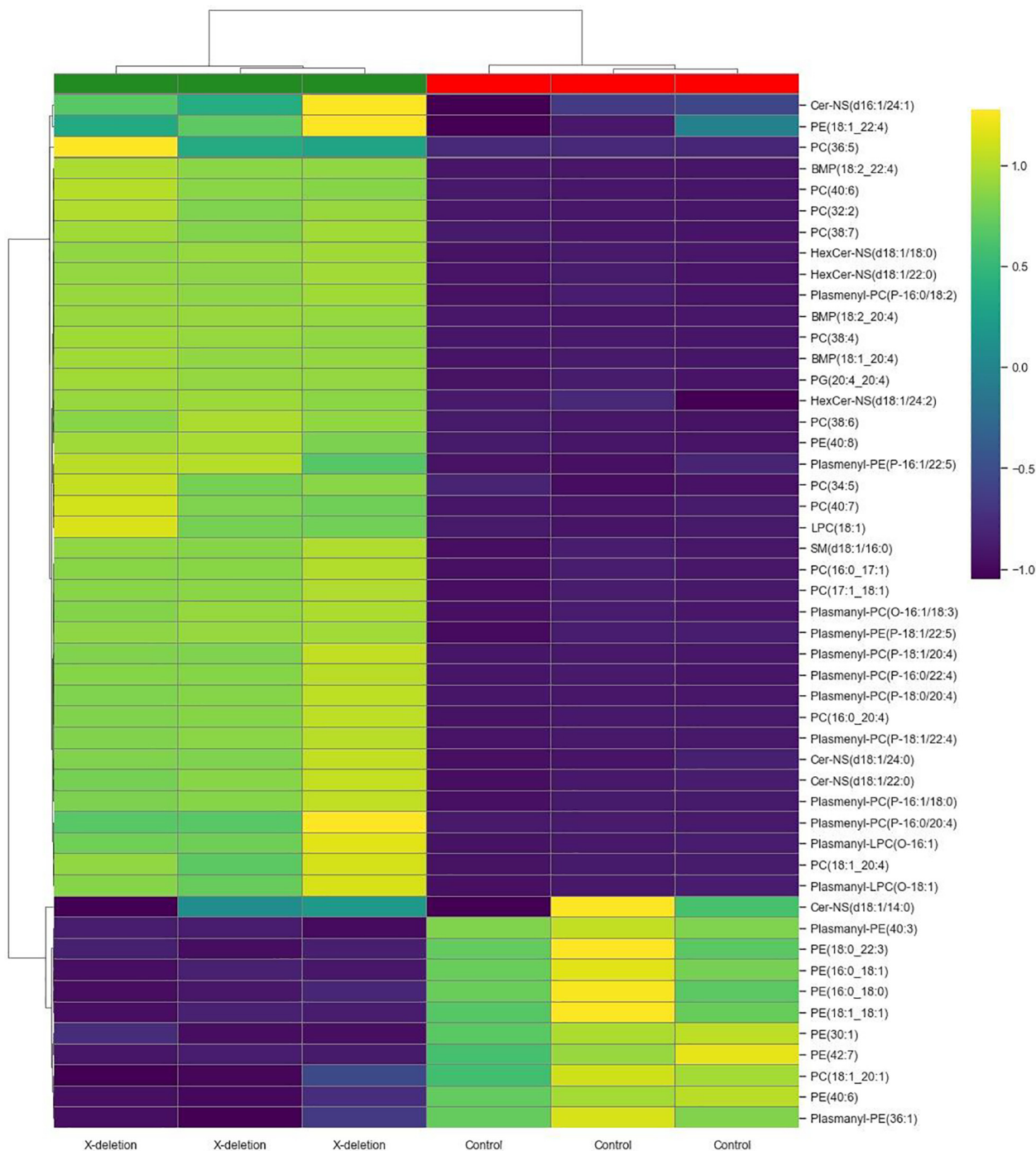


Fig. 3. Heatmap of lipid relative intensities showing hierarchical clustering of the top 50 most significant lipids from the Student's t-test analysis in positive mode (Green: X-deletion group, Red: Control group). Elucidation distance measurement and Ward clustering algorithm were used.

phospholipids of cellular membranes in humans [36]. They are required to accommodate the augmented demand for new membrane biosynthesis during neuronal differentiation [37]. PEs are the second most abundant phospholipid in mammalian membranes and are enriched in mitochondrial inner membranes [36]. Small changes in the phospholipid composition of cells can have important consequences in terms of signaling mediated by lipid derivatives. Significant alterations in some neural membrane phospholipids have been reported in neurological disorders and affect the membrane fluidity, stability, and permeability [38]. Additionally, it was found that there are few highly expressed lipid species containing very-long-chain fatty acids (VLCFA) with different

degrees of unsaturation in the X-deletion sample (such as plasmaynyl-PC(P-16:0/22:4), plasmaynyl-PC(P-18:1/22:4), plasmaynyl-PC(O-16:1/22:4), and plasmaynyl-PC(P-18:1/22:4)), in which the presence of these fatty acids is usually associated with peroxisomal β -oxidation defects and neurodegenerative disorders [39].

Fig. 4 shows a comparison of the lipid profiles for X-deletion vs control, using the sum of the intensities of all identified lipids in each group as a measure of relative total expression. The 'Other Lipids' group in this Figure includes all of the other detected lipid classes comprising a minority of the total lipid signal and are detailed in Table S3. In both X-deletion syndrome and the control,

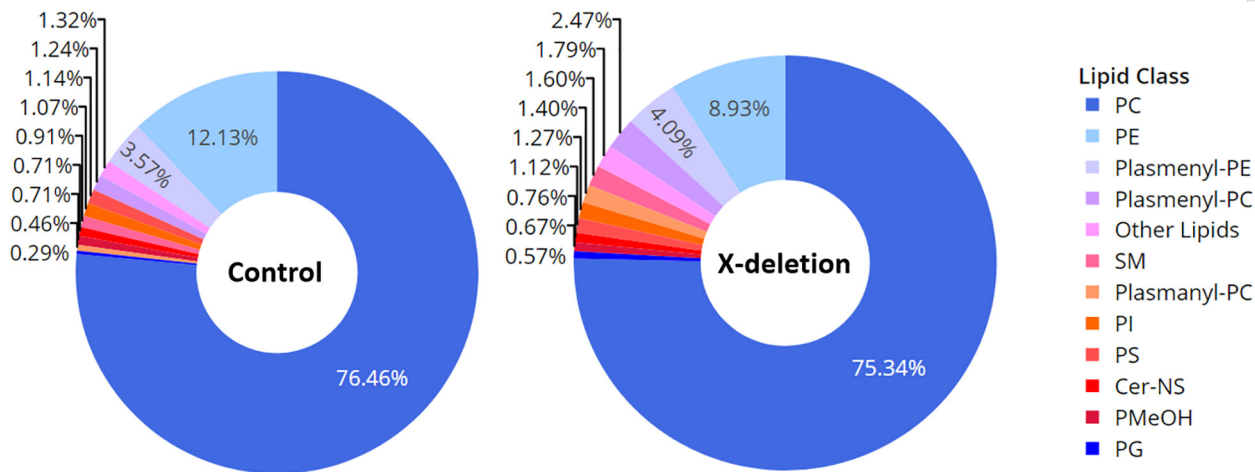


Fig. 4. Distribution of identified lipid species by summation of class intensity for control and X-deletion samples. Most lipids were determined to be phosphatidylcholines (PC), phosphatidylethanolamines (PE), plasmenyl-PE, and Plasmenyl-PC. The PC/PE ratio is different in X-deletion compared to the control (PC/PE = 8.43 versus 6.32), also plasmalogens (plasmenyl-PE, plasmenyl-PC, and plasmanyl-PC) are relatively higher in X-deletion syndrome. Other lipids group describe a minority (2% or less) of the total lipid intensity.

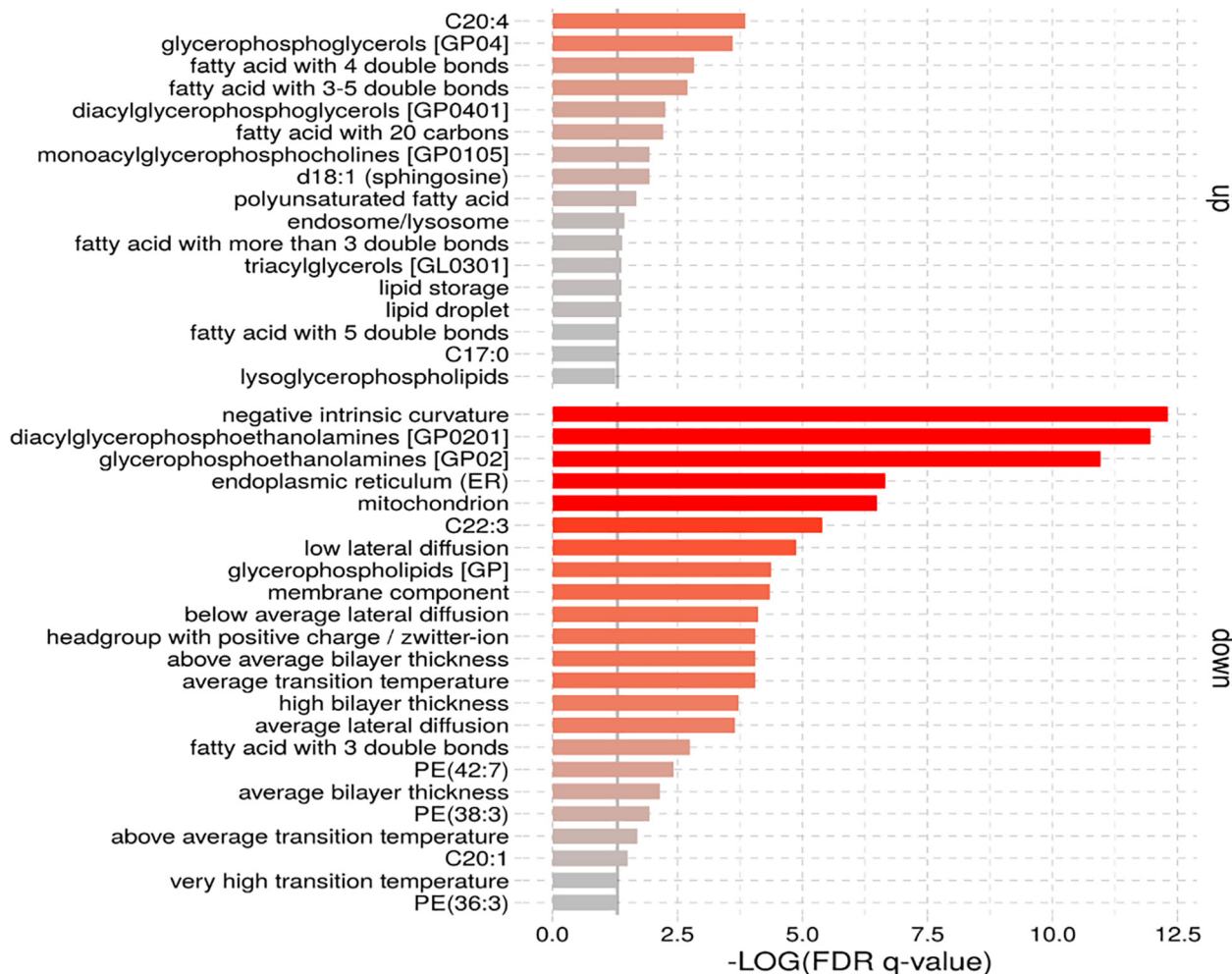


Fig. 5. Lipid enrichment analysis of X-deletion samples vs. control samples in the ranking mode. The gray vertical lines imply the cut-off value of significant enrichments ($q < 0.05$).

PC and PE had the highest-class representation with 75.34% and 8.93% in X-deletion and 76.46% and 12.13% in the control; however, the ratio of these classes as a measure of the total lipid signal

were significantly different between the X-deletion and control groups. As shown in Fig. 4, the PC/PE ratio is profoundly different in X-deletion versus control (PC/PE = 8.43 versus 6.32, Fig. S2), with

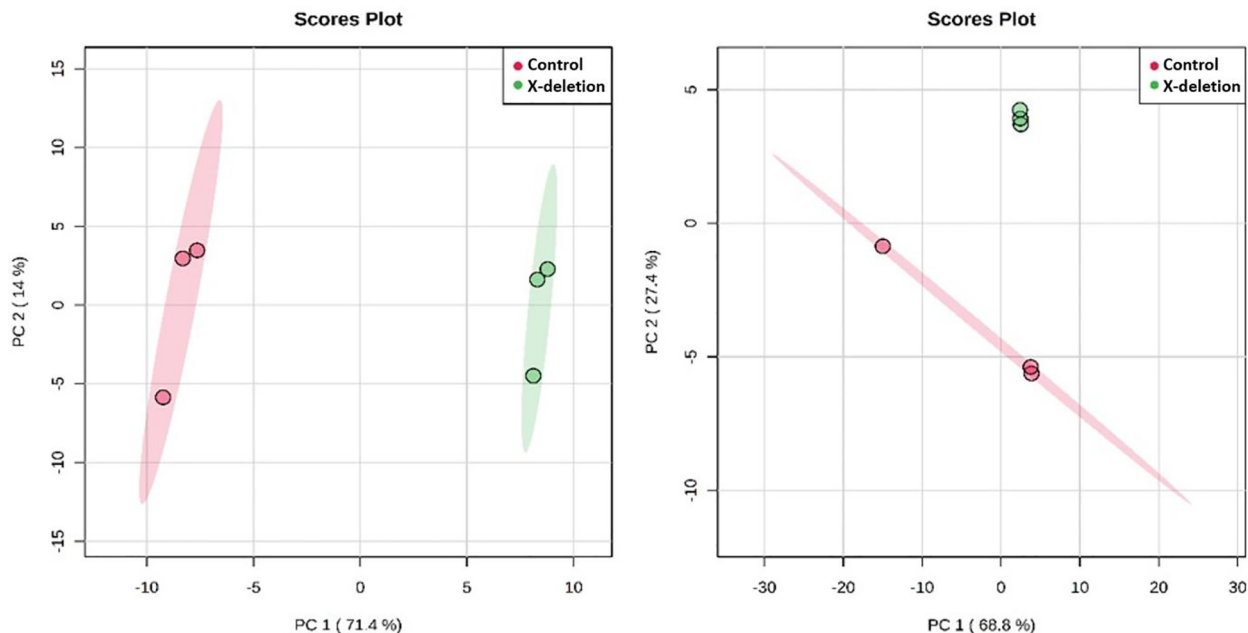


Fig. 6. The principal component analysis was constructed using metabolomics data and could separate the samples when plotted against the first two principal components (Left: positive mode, Right: negative mode).

Table 3

Mean peak height (PH) of significantly different metabolites in X-deletion (n = 3) compared to control samples (n = 3) and their ratio (ID methods: 1 = m/z match to internal library, 2 = retention time match to internal library).

Metabolite Name	m/z	Ion/Adduct	ID methods	Mass Accuracy (ppm)	Average X-deletion PH (n = 3)	X-deletion RSD (%)	Average Control PH (n = 3)	Control RSD (%)	X-deletion/Control
Glutamine (NEG)	145.0618	[M-H] ⁻	1,2	3.5	2.61E+06	9.69	5.91E+04	86.62	44.2
Dihydroxyacetone Phosphate (NEG)	168.9905	[M-H] ⁻	1,2	1.5	1.15E+06	15.03	3.81E+04	55.32	30.1
Phosphocholine (POS)	184.0735	[M+H] ⁺	1,2	-1.8	5.83E+07	0.76	3.26E+06	4.69	17.9
6-Phosphogluconic Acid (NEG)	275.0178	[M-H] ⁻	1,2	3.7	1.31E+05	20.3	8.70E+03	89.98	15
Ribulose 5-Phosphate (POS)	253.0084	[M+H] ⁺	1,2	0	2.32E+05	5.24	1.62E+04	27	14.3
D-Ribose 5-Phosphate (NEG)	229.0112	[M-H] ⁻	1,2	-0.7	1.80E+06	4.18	1.63E+05	18.87	11
Arachidonic Acid (20:4) (NEG)	303.2329	[M-H] ⁻	1,2	1.7	9.75E+05	70.8	9.12E+04	107.06	10.7
2-Aminoethyl Dihydrogen Phosphate (NEG)	140.0119	[M-H] ⁻	1,2	4.7	2.59E+06	4.69	2.89E+05	87.32	9
Docosahexaenoic Acid (22:6) (NEG)	327.233	[M-H] ⁻	1,2	1.7	1.41E+05	70.73	1.58E+04	120.27	9
CMP (NEG)	322.0443	[M-H] ⁻	1,2	1	9.20E+05	22.02	1.18E+05	86.68	7.8
Ethanolamine Phosphate (POS)	142.0263	[M+H] ⁺	1,2	4.3	8.09E+06	5.97	1.06E+06	3.72	7.6
Ascorbic Acid (NEG)	173.0085	[M-H] ⁻	1,2	-0.7	3.06E+04	19.81	2.22E+05	67.11	7.3

this higher PC/PE ratio an indicator of lipid disequilibrium. Abnormal cellular PC/PE ratios can impact energy metabolism and have been associated with disease progression. The relative abundance of PC and PE controls the size and dynamics of lipid droplets, changes energy production, and regulates cell membrane integrity [40].

Another significant difference in the sum intensities of all identified lipids were plasmalogens (plasmenyl-PE, plasmenyl-PC, and plasmanyl-PC), which were relatively higher in X-deletion syndrome (plasmenyl-PE: 4.09% vs. 3.57%, plasmenyl-PC: 2.47% vs. 1.24%, and plasmanyl-PC: 1.40% vs. 0.46%). Plasmalogens, a subgroup of ether lipids, are essential membrane components involved in vesicle fusion and membrane raft composition [41]. It has been reported that plasmalogens are usually decreased in plasma and brain tissues of neurologic disorders due to increased levels of oxidative stress [42–47]. This reverse relationship between the levels of reactive oxygen species and plasmalogens was also supported in an *in vitro* study using gene-silencing for an enzyme critical for plasmalogens biosynthesis, dihydroxyacetone phosphate-acyl transferase (DHAP-AT) [48]. On the contrary,

plasmalogens are higher in the X-deletion group in this study, suggesting a potential dysregulation of plasmalogen biosynthesis and breakdown efficiency in this specific X-deletion syndrome.

Lipid enrichment analysis in Fig. 5 clearly shows notable downregulation of negative intrinsic curvature, PE biosynthesis, endoplasmic reticulum, and mitochondrion lipid metabolism, as well as upregulation of long-chain polyunsaturated fatty acids (PUFAs) and PG metabolism in X-deletion samples. Negative intrinsic curvature relates to the cellular membrane shape and a negative curvature indicates that the cell membrane protrudes inward [49]. Lipids like PE that have relatively large hydrophobic tails and small polar headgroups form an almost conical shape, which imposes the intrinsic negative curvature [50]. The downregulation of intrinsic negative curvature lipid metabolism in the X-deletion group corresponds to the prior result of lower PE lipids compared to control.

Studies have indicated that long-chain PUFAs play an essential role in normal brain growth and cognitive development in infants [51–53]. The dysregulation of PUFAs in X-deletion samples could be a critical element in brain function in this patient and for X-deletion syndrome. Thus, changes in PUFAs lipid metabolism could

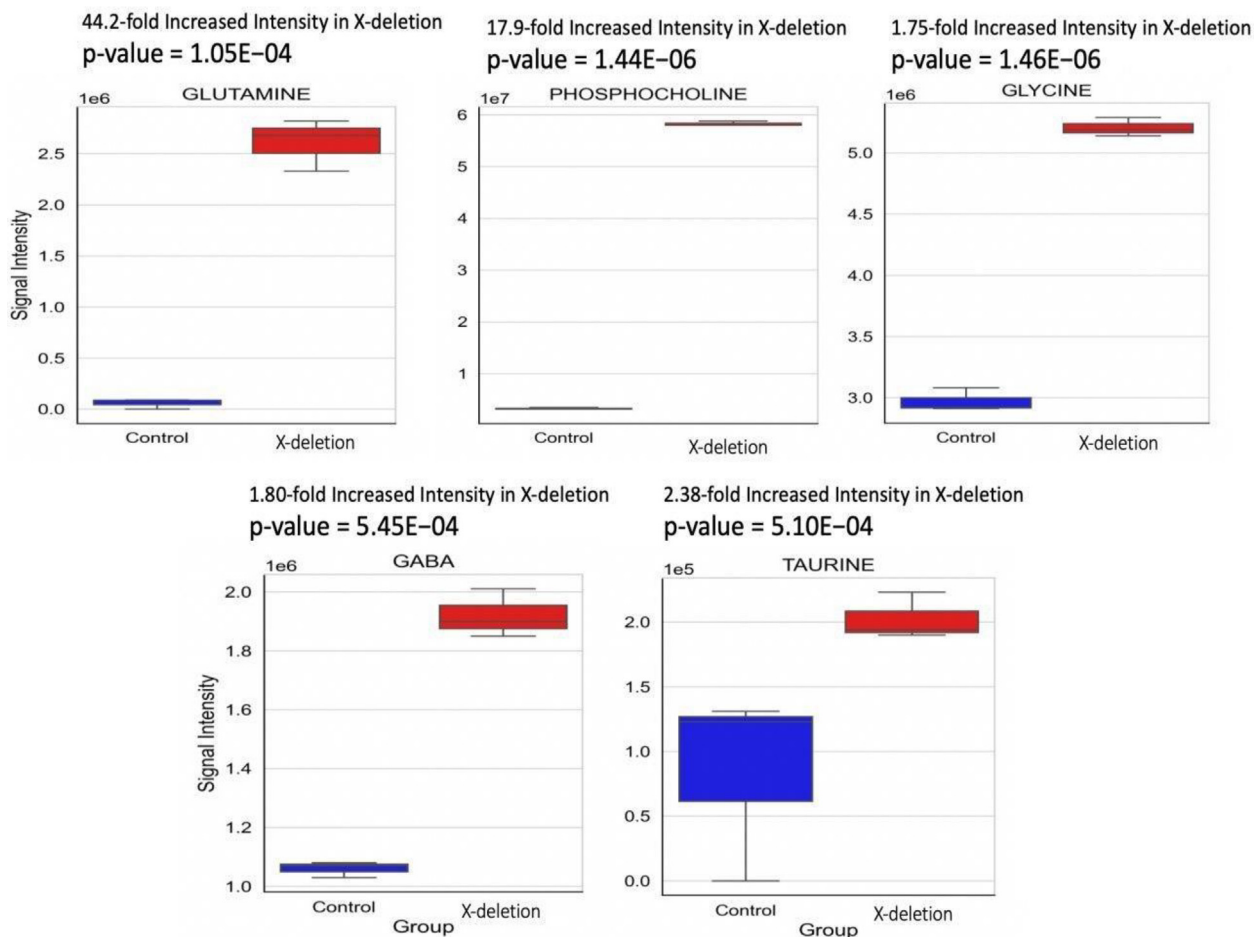


Fig. 7. Box plots showing significant metabolites, which are related to neurotransmitters, their precursors, or catabolites.

be considered a target for future therapies. In total, these results indicate a significant alteration in phospholipid metabolism in X-deletion syndrome, resulting in possible abnormalities in energy metabolism, feasible disruptions in protein-lipid interactions, and changes in membrane composition. Further studies are needed to determine the biological significance in the differences observed between the X-deletion and the control groups' lipidomic profiles to potentially develop therapeutic strategies.

3.2. Metabolomics analysis

Global metabolomic analysis on control and X-deletion samples generated features in positive and negative ion mode. The features were identified based on retention time and m/z using in-house libraries. 125 features in positive and 82 features in negative ion mode were identified, but, as is common in global metabolomics, a significant number of features remained unassigned. Only the identified features were used for statistical analysis. As with the lipidomics analysis, significant differences among the metabolome profiles of X-deletion and control groups were observed in the metabolomics study. Fig. 6 demonstrates a clear separation of these two groups by PCA for positive and negative ion datasets. It also shows the primary clustering of the two groups along PC1 in both ion modes, explaining 85.4% of the variance in 2 PCs in positive and 96.2% of the variance in negative ion mode. Table 3 presents information about the top 12 significantly identified metabolites with fold changes greater than 7.5 in positive and negative ion modes (focusing on lipids with the highest magnitude of change). The most significant metabolite identified was glutamine,

with a 44.2-fold increased intensity in the X-deletion sample and a p-value of 1.05E-04. Glutamine has a prolific presence in the nervous system, where it participates in a variety of metabolic pathways. Its primary role is that of a precursor to the neurotransmitter amino acids: the excitatory amino acids, aspartate, glutamate, and the inhibitory amino acid, γ -aminobutyric acid (GABA) [54]. Research studying animal models of FXS, characterized by limited or lack of fragile X mental retardation protein (FMRP), has associated brain dysfunction with a dysregulation in the glutamatergic and cholinergic systems [55]. Studies also report that drugs employed to treat excessive glutamine and its signaling pathways affected by FMRP are under different stages of development in FXS [56]. Phosphocholine (17.9-fold increased intensity in the X-deletion sample and a p-value of 1.44E-06) also showed excellent representation among the significant metabolites in Table 3. Phosphocholine is the precursor choline, a key neurotransmitter. Choline is required for healthy brain development and has pivotal functions in the modulation of cholinergic neurotransmission, which is often dysregulated in some neurodegenerative disorders [57]. In addition, the upregulation of choline has been reported in the brain of FXS mouse models [11]. Phosphocholine is also a precursor of phosphatidylcholine (PC) lipids [58] and its abundance in X-deletion samples corresponds to the prior result of a higher intensity of some PC lipid species in this group as compared to control, as described in the previous section. Results in this study have revealed that NPs from X-deletion samples have dramatic impacts on the level of neurotransmitters, their precursors, or catabolites. Other significant metabolites related to the X-deletion group that are related to neurotransmitters include

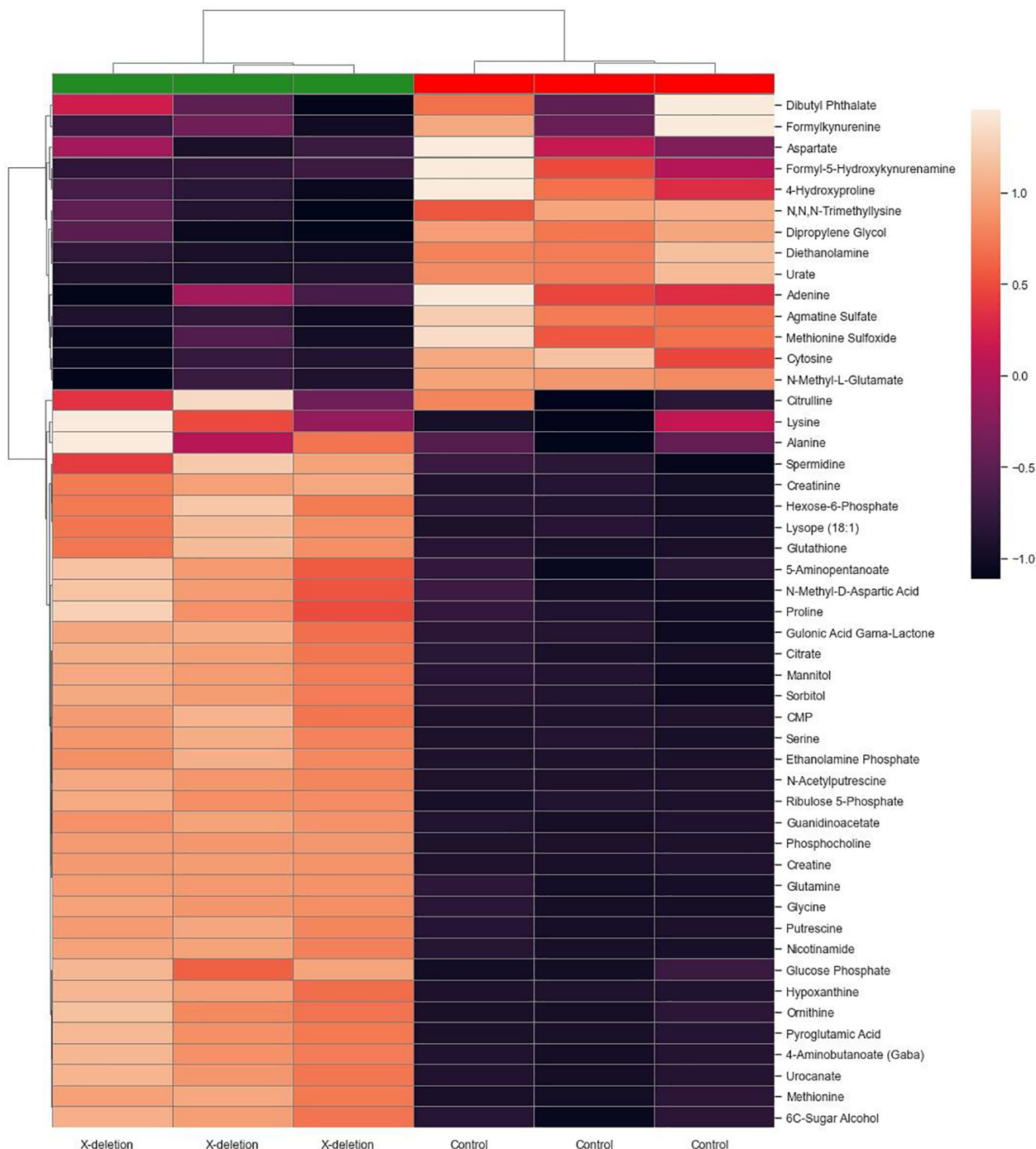


Fig. 8. Heatmap of metabolite relative intensities showing hierarchical clustering of the top 50 most significant metabolites from the Student's *t*-test analysis in positive mode (Green: X-deletion group, Red: Control group). Elucidation distance measurement and Ward clustering algorithm were used.

glycine (1.75-fold, p -value = $1.46E-06$), γ -aminobutyric acid (GABA) (1.80-fold, p -value = $5.45E-04$), and taurine (2.38-fold, p -value = $5.10E-04$) all with increased intensity in X-deletion (Fig. 7). Such differential expression of these key neurotransmitters could have a variety of biological implications and no other related reports have focused on these compounds, thus, they warrant further investigation.

Hierarchical clustering analysis of the metabolites in positive ion mode is shown in Fig. 8, with results of the same analysis in negative ion mode shown in Fig. S3, depicting the changes of the top 50 most significant metabolites from the Student's *t*-test anal-

ysis in the X-deletion sample as compared to the control. Shades of orange and purple represent an increased or decreased fold change, respectively, of a metabolite in the X-deletion sample relative to control. Significant hierarchical clustering groups were observed among the cells and metabolites were found to be mostly higher in intensity in the X-deletion sample. Interestingly, many of the other significantly identified metabolites, as shown in the positive and negative ion mode heatmaps, were found to be nucleosides, nucleotides, or their derivatives, such as guanine (2.17-fold, p -value = $2.61E-04$), cytidine (2.16-fold, p -value = $7.37E-04$), adenine (1.41-fold, p -value = $2.72E-04$), and guanosine (1.83-fold, p -valu

$e = 1.20E-04$). Also, ribulose 5-phosphate, a precursor for the synthesis of nucleotides in the pentose phosphate pathway was significantly higher in the X-deletion sample with 14.3-fold higher intensity and a p-value of $6.98E-05$. Dysfunction of the pentose phosphate pathway has been reported in neuroinflammation and neurodegeneration *in vitro* and *in vivo* [59]. Furthermore, a selection of metabolites of N-acetylated species are also present in the heatmaps with higher intensities in X-deletion samples, including N-acetylputrescine (5.36-fold higher intensity in X-deletion), N-acetylaspartylglutamic acid (3.84-fold higher intensity in X-deletion), and N-acetylneuraminic acid (2.7-fold higher intensity in X-deletion). Previous studies have shown that N-acetylated species such as N-acetylputrescine are dysregulated in some neurodegenerative diseases [60,61].

After hierarchical clustering analysis, we performed metabolite set enrichment analysis (MSEA) on differential metabolites (p-value <0.05) screened in the X-deletion and control samples. MSEA describes that the deleted genes in X-deletion disturbed the metabolic regulation network severely (Fig. 9A). This result indicates that the intensities of several amino acids and their metabolites were significantly changed in X-deletion. These are mainly involved in glutathione, alanine, aspartate, glutamate, glycine, serine, threonine, methionine, arginine, proline, and glutamate metabolism and homocysteine degradation. Furthermore, metabolome view analysis was also performed on differential metabolites (p-value < 0.05) to confirm whether a metabolite node was affected or not (Fig. 9B). As is shown in Fig. 9B, arginine and proline metabolism had one of the lowest p-values ($1.74E-06$), and one of the highest pathway impact scores. Arginine is among the most metabolically versatile amino acids and its metabolism in the brain is essential for normal brain function [48]. In addition to brain protein synthesis, arginine is a precursor

for the synthesis of ornithine, urea, creatine, nitric oxide, agmatine, polyamines, glutamic acid, and proline [62–64]. Previous studies have suggested that the arginine-rich dipeptides, particularly, Proline-Arginine (PR), are extremely neurotoxic and imply translational dysregulation. A much higher risk of degeneration was observed in neurons with nuclear PR aggregates confirming potential neurotoxicity of the PR dipeptide when expressed *in vivo* [65]. Therefore, the dysregulation of the arginine and proline metabolism could change several other amino acid metabolic pathways and be responsible for various symptoms of the X-deletion disorder. The manually constructed metabolic network (Fig. 9C) clearly shows that the deleted genes can potentially be related to the alterations in the tricarboxylic acid cycle, arginine and proline metabolism, glutathione metabolism, glycine, serine, and threonine metabolism, alanine, aspartate, and glutamate metabolism. Further work is required to confirm the biological functionality of these presented metabolites, as well as all other metabolites identified in this research, and characterize the reason for their differential expression between X-deletion and control samples.

4. Conclusion

In this study, we observed that the lipidomic and metabolomic profiles of X-deletion and control NP cells exhibited significant differentiation associated with partial deletion of the X chromosome involving several neurotransmitters, nucleosides, glycerophospholipids, and the readjustment of brain biochemical pathways. Lipidomic and Metabolomic pathway analysis revealed that several pathways are potentially dysregulated in X-deletion samples, including negative intrinsic curvature, PE lipid metabolism, as well

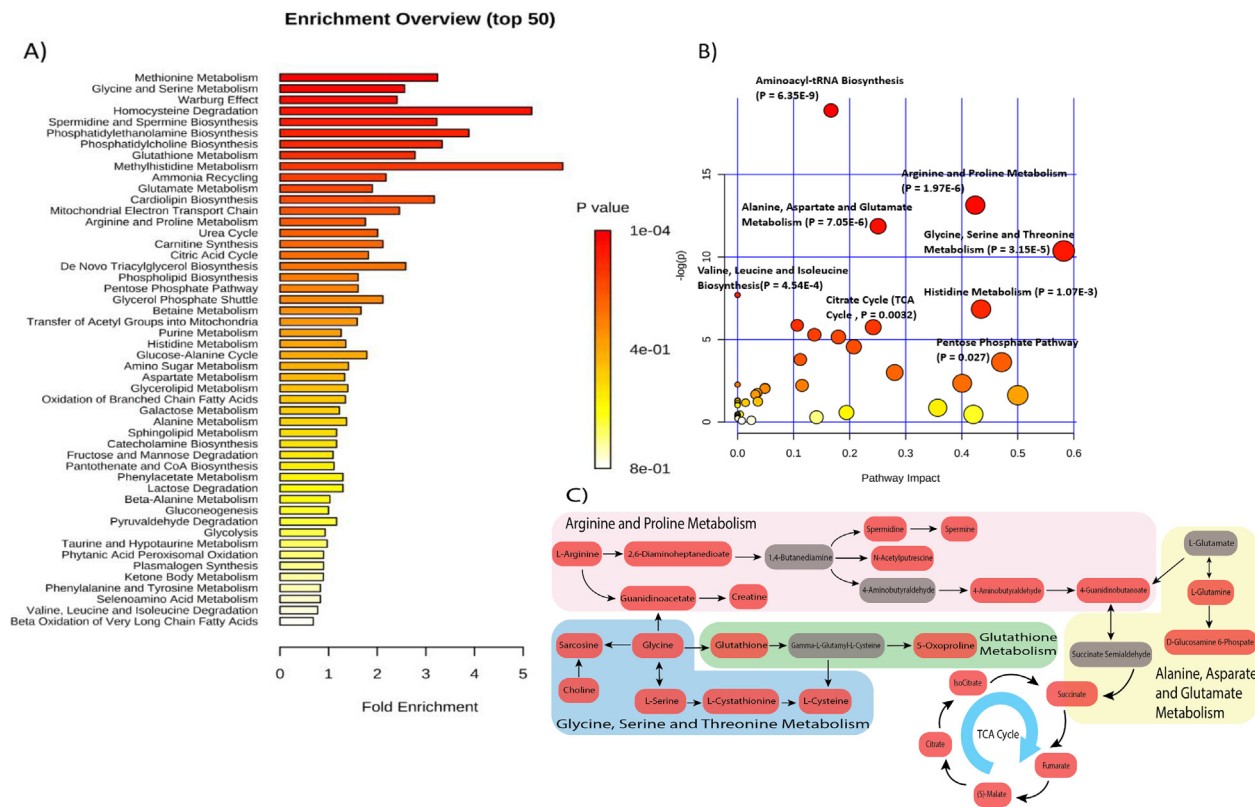


Fig. 9. A) Metabolomic Pathway Analysis (MetPA) as generated by the MetaboAnalyst software package and ranked by Holm p-value. B) All the paired pathways are presented as circles. The color of each circle is based on p-values from pathway enrichment analysis and the size of the circle represents the metabolic pathway impact score calculated from pathway topology analysis. The most impacted metabolic pathways having important statistical significance scores are annotated. C) Metabolic network associated with the differential metabolites identified in the X-deletion group. Metabolites colored in red are upregulated metabolites in X-deletion samples.

as arginine and proline metabolism, glutathione metabolism, glycine, serine, and threonine metabolism, and alanine, aspartate, and glutamate metabolism. These findings define that rare X-deletion disorders are not only a mental disorder limited to alterations in local neuronal functions, but are also a metabolic disease. This study provides possible explanations for the symptoms of X-deletion disorder patients and provides additional information for better understanding this rare syndrome. Additional work is needed to determine the biological and pathological relevance of the differential expression of significant compounds discussed in this work.

Conflicts of Interest

None of the authors has any conflicts of interest to disclose.

Acknowledgments

The authors gratefully acknowledge the financial support of the Xtraordinary Joy Foundation for which this work would not be possible.

Appendix A. Supplementary data

Supplementary data to this article can be found online at <https://doi.org/10.1016/j.jmsacl.2021.05.002>.

References

- [1] H.A. Lubs, R.E. Stevenson, C.E. Schwartz, Fragile X and X-linked intellectual disability: four decades of discovery, *Am. J. Hum. Genet.* 90 (4) (2012) 579–590.
- [2] R.E. Stevenson, C.E. Schwartz, X-linked intellectual disability: unique vulnerability of the male genome, *Dev. Disabil. Res. Rev.* 15 (4) (2009) 361–368.
- [3] T. Ogata, K. Muroya, N. Matsuo, O. Shinohara, T. Yorifuji, Y. Nishi, Y. Hasegawa, R. Horikawa, K. Tachibana, Turner syndrome and Xp deletions: clinical and molecular studies in 47 patients, *J. Clin. Endocrinol. Metab.* 86 (11) (2001) 5498–5508.
- [4] S.J. Rogers, D.E. Wehner, R. Hagerman, The behavioral phenotype in fragile X: symptoms of autism in very young children with fragile X syndrome, idiopathic autism, and other developmental disorders, *J. Dev. Behav. Pediatr.* 22 (6) (2001) 409–417.
- [5] K. Dettmer, P.A. Aronov, B.D. Hammock, Mass spectrometry-based metabolomics, *Mass Spectrom. Rev.* 26 (1) (2007) 51–78.
- [6] W.B. Dunn, D.I. Ellis, Metabolomics: current analytical platforms and methodologies, *Trac-Trend Anal. Chem.* 24 (4) (2005) 285–294.
- [7] M.R. Wenk, The emerging field of lipidomics, *Nat. Rev. Drug Discov.* 4 (7) (2005) 594–610.
- [8] R.E. Gerszten, T.J. Wang, The search for new cardiovascular biomarkers, *Nature* 451 (7181) (2008) 949–952.
- [9] C.H. Johnson, J. Ivanisevic, G. Siuzdak, Metabolomics: beyond biomarkers and towards mechanisms, *Nat. Rev. Mol. Cell Biol.* 17 (7) (2016) 451–459.
- [10] J.C. Naviaux, L. Wang, K.F. Li, A.T. Bright, W.A. Alaynick, K.R. Williams, S.B. Powell, R.K. Naviaux, Antipurinergic therapy corrects the autism-like features in the Fragile X (Fmr1 knockout) mouse model, *Mol. Autism* 6 (2015).
- [11] L. Davidovic, V. Navratil, C.M. Bonaccorso, M.V. Catania, B. Bardoni, M.E. Dumas, A metabolomic and systems biology perspective on the brain of the Fragile X syndrome mouse model, *Genome Res.* 21 (12) (2011) 2190–2202.
- [12] K.E. Ginton, S.H. Elsea, Untargeted metabolomics for autism spectrum disorders: current status and future directions, *Front. Psychiatry* 10 (2019).
- [13] J. Bugajska, J. Berska, M. Wojcik, J.B. Starzyk, K. Sztefko, Metabolic fingerprint of Turner syndrome, *J. Clin. Med.* 9 (3) (2020).
- [14] H. Wang, Modeling neurological diseases with human brain organoids, *Front. Synaptic Neurosci.* 10 (2018) 15.
- [15] X.Y. Qin, H. Akanuma, F.F. Wei, R. Nagano, Q. Zeng, S. Imanishi, S. Ohsako, J. Yoshinaga, J. Yonemoto, M. Tanokura, H. Sone, Effect of low-dose thalidomide on dopaminergic neuronal differentiation of human neural progenitor cells: A combined study of metabolomics and morphological analysis, *Neurotoxicology* 33 (5) (2012) 1375–1380.
- [16] N. Watanabe, K. Kitada, K.E. Santostefano, A. Yokoyama, S.M. Waldrop, C.D. Heldermon, D. Tachibana, M. Koyama, A.M. Meacham, C.A. Pacak, N. Terada, Generation of induced pluripotent stem cells from a female patient with a Xq27.3-q28 deletion to establish disease models and identify therapies, *Cell Reprogram* (2020).
- [17] J. Folch, M. Lees, G.H. Sloane Stanley, A simple method for the isolation and purification of total lipids from animal tissues, *J. Biol. Chem.* 226 (1) (1957) 497–509.
- [18] J.P. Koelmel, N.M. Kroeger, E.L. Gill, C.Z. Ulmer, J.A. Bowden, R.E. Patterson, R.A. Yost, T.J. Garrett, Expanding lipidome coverage using LC-MS/MS data-dependent acquisition with automated exclusion list generation, *J. Am. Soc. Mass Spectr.* 28 (5) (2017) 908–917.
- [19] L. He, J. Diedrich, Y.Y. Chu, J.R. Yates 3rd, Extracting accurate precursor information for tandem mass spectra by RawConverter, *Anal. Chem.* (2015), 87 (22), 11361–7.
- [20] T. Pluskal, S. Castillo, A. Villar-Briones, M. Oresic, MZmine 2: modular framework for processing, visualizing, and analyzing mass spectrometry-based molecular profile data, *BMC Bioinf.* 11 (2010) 395.
- [21] L.W. Sumner, A. Amberg, D. Barrett, M.H. Beale, R. Beger, C.A. Daykin, T.W. Fan, O. Fiehn, R. Goodacre, J.L. Griffin, T. Hankemeier, N. Hardy, J. Harnly, R. Higashi, J. Kopka, A.N. Lane, J.C. Lindon, P. Marriott, A.W. Nicholls, M.D. Reilly, J.J. Thaden, M.R. Viant, Proposed minimum reporting standards for chemical analysis Chemical Analysis Working Group (CAWG) Metabolomics Standards Initiative (MSI), *Metabolomics* 3 (3) (2007) 211–221.
- [22] J.P. Koelmel, N.M. Kroeger, C.Z. Ulmer, J.A. Bowden, R.E. Patterson, J.A. Cochran, C.W.W. Beecher, T.J. Garrett, R.A. Yost, LipidMatch: an automated workflow for rule-based lipid identification using untargeted high-resolution tandem mass spectrometry data, *BMC Bioinf.* 18 (2017).
- [23] J. Chong, O. Soufan, C. Li, I. Caraus, S. Li, G. Bourque, D.S. Wishart, J. Xia, MetaboAnalyst 4.0: towards more transparent and integrative metabolomics analysis, *Nucleic Acids Res.* 46 (W1) (2018) W486–W494.
- [24] K.J. Millman, M. Aivazis, Python for scientists and engineers, *Comput. Sci. Eng.* 13 (2) (2011) 9–12.
- [25] M.R. Molenaar, A. Jeucken, T.A. Wassenaar, C.H.A. van de Lest, J.F. Brouwers, J.B. Helms, LION/web: a web-based ontology enrichment tool for lipidomic data analysis, *GigaScience* 8 (6) (2019).
- [26] D.S. Wishart, D. Tzur, C. Knox, R. Eisner, A.C. Guo, N. Young, D. Cheng, K. Jewell, D. Arndt, S. Sawhney, C. Fung, L. Nikolai, M. Lewis, M.A. Coutouly, I. Forsythe, P. Tang, S. Shrivastava, K. Jeroncic, P. Stothard, G. Amegbey, D. Block, D.D. Hau, J. Wagner, J. Miniaci, M. Clements, M. Gebremedhin, N. Guo, Y. Zhang, G.E. Duggan, G.D. Macinnis, A.M. Weljie, R. Dowlatabadi, F. Bamforth, D. Clive, R. Greiner, L. Li, T. Marrie, B.D. Sykes, H.J. Vogel, L. Querengesser, HMDB: The Human Metabolome Database, *Nucleic Acids Res.* 35 (Database issue) (2007) D521–D526.
- [27] D.S. Wishart, C. Knox, A.C. Guo, R. Eisner, N. Young, B. Gautam, D.D. Hau, N. Psychogios, E. Dong, S. Bouatra, R. Mandal, I. Sinelnikov, J. Xia, L. Jia, J.A. Cruz, E. Lim, C.A. Sobsey, S. Shrivastava, P. Huang, P. Liu, L. Fang, J. Peng, R. Fradette, D. Cheng, D. Tzur, M. Clements, A. Lewis, A. De Souza, A. Zuniga, M. Dawe, Y. Xiong, D. Clive, R. Greiner, A. Nazyrova, R. Shaykhtudinov, L. Li, H.J. Vogel, I. Forsythe, HMDB: a knowledgebase for the human metabolome, *Nucleic Acids Res.* 37 (Database issue) (2009) D603–D610.
- [28] D.S. Wishart, T. Jewison, A.C. Guo, M. Wilson, C. Knox, Y. Liu, Y. Djoumbou, R. Mandal, F. Aziat, E. Dong, S. Bouatra, I. Sinelnikov, D. Arndt, J. Xia, P. Liu, F. Yallou, T. Bjorn Dahl, R. Perez-Pineiro, R. Eisner, F. Allen, V. Neveu, R. Greiner, A. Scalbert, HMDB 3.0—The Human Metabolome Database in 2013, *Nucleic Acids Res.* 41 (Database issue) (2013) D801–D807.
- [29] D.S. Wishart, Y.D. Feunang, A. Marcu, A.C. Guo, K. Liang, R. Vázquez-Fresno, T. Sajed, D. Johnson, C. Li, N. Karu, Z. Sayeeda, E. Lo, N. Assempour, M. Berjanskii, S. Singhal, D. Arndt, Y. Liang, H. Badran, J. Grant, A. Serra-Cayuela, Y. Liu, R. Mandal, V. Neveu, A. Pon, C. Knox, M. Wilson, C. Manach, A. Scalbert, HMDB 4.0: the human metabolome database for 2018, *Nucleic Acids Res.* 46 (D1) (2018) D608–D617.
- [30] S. Kim, J. Chen, T. Cheng, A. Gindulyte, J. He, S. He, Q. Li, B.A. Shoemaker, P.A. Thiessen, B. Yu, L. Zaslavsky, J. Zhang, E.E. Bolton, PubChem 2019 update: improved access to chemical data, *Nucleic Acids Res.* 47 (D1) (2019) D1102–D1109.
- [31] J. Wixon, D. Kell, The Kyoto encyclopedia of genes and genomes—KEGG, *Yeast* 17 (1) (2000) 48–55.
- [32] M. Kanehisa, Toward understanding the origin and evolution of cellular organizations, *Protein Sci.* 28 (11) (2019) 1947–1951.
- [33] M. Kanehisa, M. Furumichi, Y. Sato, M. Ishiguro-Watanabe, M. Tanabe, KEGG: integrating viruses and cellular organisms, *Nucleic Acids Res.* (2020).
- [34] Y. Djoumbou-Feunang, A. Pon, N. Karu, J.M. Zheng, C. Li, D. Arndt, M. Gautam, F. Allen, D.S. Wishart, CFM-ID 3.0: Significantly Improved ESI-MS/MS Prediction and Compound Identification, *Metabolites* 9 (4) (2019).
- [35] N.G. Mahieu, G.J. Patti, Systems-level annotation of a metabolomics data set reduces 25 000 features to fewer than 1000 unique metabolites, *Anal. Chem.* 89 (19) (2017) 10397–10406.
- [36] Z.Y. Li, L.B. Agellon, T.M. Allen, M. Umeda, L. Jewel, A. Mason, D.E. Vance, The ratio of phosphatidylcholine to phosphatidylethanolamine influences membrane integrity and steatohepatitis, *Cell Metab.* 3 (5) (2006) 321–331.
- [37] H. Marcucci, L. Paoletti, S. Jackowski, C. Banchio, Phosphatidylcholine biosynthesis during neuronal differentiation and its role in cell fate determination, *J. Biol. Chem.* 285 (33) (2010) 25382–25393.
- [38] A.A. Farooqui, L.A. Horrocks, T. Farooqui, Glycerophospholipids in brain: their metabolism, incorporation into membranes, functions, and involvement in neurological disorders, *Chem. Phys. Lipids* 106 (1) (2000) 1–29.
- [39] S. Kemp, F. Valianpour, S. Denis, R. Ofman, R.J. Sanders, P. Mooyer, P.G. Barth, R.J.A. Wanders, Elongation of very long-chain fatty acids is enhanced in X-linked adrenoleukodystrophy, *Mol. Genet. Metab.* 84 (2) (2005) 144–151.

- [40] J.N. van der Veen, J.P. Kennelly, S. Wan, J.E. Vance, D.E. Vance, R.L. Jacobs, The critical role of phosphatidylcholine and phosphatidylethanolamine metabolism in health and disease, *Biochim. Biophys. Acta Biomembr.* 1859 (9) (2017) 1558–1572.
- [41] F. Dorninger, S. Forss-Petter, J. Berger, From peroxisomal disorders to common neurodegenerative diseases - the role of ether phospholipids in the nervous system, *FEBS Lett.* 591 (18) (2017) 2761–2788.
- [42] E.J. Murphy, M.B. Schapiro, S.I. Rapoport, H.U. Shetty, Phospholipid composition and levels are altered in Down syndrome brain, *Brain Res.* 867 (1–2) (2000) 9–18.
- [43] R.H. Thomas, K.A. Foley, J.R. Mephram, L.J. Tichenoff, F. Possmayer, D.F. MacFabe, Altered brain phospholipid and acylcarnitine profiles in propionic acid infused rodents: further development of a potential model of autism spectrum disorders, *J. Neurochem.* 113 (2) (2010) 515–529.
- [44] M. Khan, J. Singh, I. Singh, Plasmalogen deficiency in cerebral adrenoleukodystrophy and its modulation by lovastatin, *J. Neurochem.* 106 (4) (2008) 1766–1779.
- [45] E. Miville-Godbout, M. Bourque, M. Morissette, S. Al-Sweidi, T. Smith, A. Mochizuki, V. Senanayake, D. Jayasinghe, L. Wang, D. Goodenowe, T. Di Paolo, Plasmalogen augmentation reverses striatal dopamine loss in MPTP mice, *PLoS ONE* 11 (3) (2016).
- [46] N. Fabelo, V. Martin, R. Marin, G. Santpere, E. Aso, I. Ferrer, M. Diaz, Evidence for premature lipid raft aging in APP/PS1 double-transgenic mice, a model of familial Alzheimer disease, *J. Neuropath. Exp. Neur.* 71 (10) (2012) 868–881.
- [47] Y. Tajima, M. Ishikawa, K. Maekawa, M. Murayama, Y. Senoo, T. Nishimaki-Mogami, H. Nakanishi, K. Ikeda, M. Arita, R. Taguchi, A. Okuno, R. Mikawa, S. Niida, O. Takikawa, Y. Saito, Lipidomic analysis of brain tissues and plasma in a mouse model expressing mutated human amyloid precursor protein/tau for Alzheimer's disease, *Lipids Health Dis.* 12 (2013).
- [48] D. Reiss, K. Beyer, B. Engelmann, Delayed oxidative degradation of polyunsaturated diacyl phospholipids in the presence of plasmalogen phospholipids in vitro, *Biochem. J.* 323 (Pt 3) (1997) 807–814.
- [49] I.K. Jarsch, F. Daste, J.L. Gallop, Membrane curvature in cell biology: An integration of molecular mechanisms, *J. Cell Biol.* 214 (4) (2016) 375–387.
- [50] H.T. McMahon, E. Boucrot, Membrane curvature at a glance, *J. Cell Sci.* 128 (6) (2015) 1065–1070.
- [51] A. Gil, M. Ramirez, M. Gil, Role of long-chain polyunsaturated fatty acids in infant nutrition, *Eur. J. Clin. Nutr.* 57 (Suppl 1) (2003) S31–S34.
- [52] S. Klevebro, S.E. Juul, T.R. Wood, A more comprehensive approach to the neuroprotective potential of long-chain polyunsaturated fatty acids in preterm infants is needed-should we consider maternal diet and the n-6:n-3 fatty acid ratio?, *Front. Pediatr.* 7 (2020).
- [53] P. Willatts, J.S. Forsyth, The role of long-chain polyunsaturated fatty acids in infant cognitive development, *Prostaglandins Leukot. Essent. Fatty Acids* 63 (1–2) (2000) 95–100.
- [54] J. Albrecht, M. Sidoryk-Wegrzynowicz, M. Zielinska, M. Aschner, Roles of glutamine in neurotransmission, *Neuron Glia Biol.* 6 (4) (2010) 263–276.
- [55] J.L. Bruno, E.W. Shelly, E.M. Quintin, M. Rostami, S. Patnaik, D. Spielman, D. Mayer, M. Gu, A.A. Lightbody, A.L. Reiss, Aberrant basal ganglia metabolism in fragile X syndrome: a magnetic resonance spectroscopy study, *J. Neurodev. Disord.* 5 (1) (2013) 20.
- [56] M.H. Davenport, T.L. Schaefer, K.J. Friedmann, S.E. Fitzpatrick, C.A. Erickson, Pharmacotherapy for Fragile X Syndrome: progress to date, *Drugs* 76 (4) (2010) 431–445.
- [57] R.A. Bekdash, Choline, the brain and neurodegeneration: insights from epigenetics, *Front. Biosci. (Landmark Ed.)* 23 (2018) 1113–1143.
- [58] J.T. Wong, M. Chan, D. Lee, J.Y. Jiang, M. Skrzypczak, P.C. Choy, Phosphatidylcholine metabolism in human endothelial cells: modulation by phosphocholine, *Mol. Cell. Biochem.* 207 (1–2) (2000) 95–100.
- [59] D. Tu, Y. Gao, R. Yang, T. Guan, J.S. Hong, H.M. Gao, The pentose phosphate pathway regulates chronic neuroinflammation and dopaminergic neurodegeneration, *J. Neuroinflammation* 16 (1) (2019) 255.
- [60] U.V. Mahajan, V.R. Varma, M.E. Griswold, C.T. Blackshear, Y. An, A.M. Oommen, S. Varma, J.C. Troncoso, O. Pletnikova, R. O'Brien, T.J. Hohman, C. Legido-Quigley, M. Thambisetty, Dysregulation of multiple metabolic networks related to brain transmethylation and polyamine pathways in Alzheimer disease: A targeted metabolomic and transcriptomic study, *PLoS Med.* 17 (1) (2020) e1003012.
- [61] S.F. Graham, O.P. Chevallier, C.T. Elliott, C. Hölscher, J. Johnston, B. McGuinness, P.G. Kehoe, A.P. Passmore, B.D. Green, Untargeted metabolomic analysis of human plasma indicates differentially affected polyamine and L-arginine metabolism in mild cognitive impairment subjects converting to Alzheimer's disease, *PLoS ONE* 10 (3) (2015) e0119452.
- [62] J. Nikolic, G. Bjelakovic, I. Stojanovic, Effect of caffeine on metabolism of L-arginine in the brain, *Mol. Cell. Biochem.* 244 (1) (2003) 125–128.
- [63] C. Lameu, A.C. de Camargo, M. Faria, L-arginine signalling potential in the brain: the peripheral gets central, *Recent Pat. CNS Drug Discov.* 4 (2) (2009) 137–142.
- [64] P. Liu, Y. Jing, N.D. Collie, B. Dean, D.K. Bilkey, H. Zhang, Altered brain arginine metabolism in schizophrenia, *Transl. Psychiat.* 6 (2016).
- [65] X.M. Wen, W.Z. Tan, T. Westergard, K. Krishnamurthy, S.S. Markandaiah, Y.X. Shi, S.Y. Lin, N.A. Shneider, J. Monaghan, U.B. Pandey, P. Pasinelli, J.K. Ichida, D. Trotti, Antisense proline-arginine RAN dipeptides linked to C9ORF72-ALS/FTD form toxic nuclear aggregates that initiate in vitro and in vivo neuronal death, *Neuron* 84 (6) (2014) 1213–1225.